Supporting Information

Electric Field-Induced Amplification of Graphene Oxide's Visible Light Photocatalytic Activity

Alsu G. Nugmanova, Maxim R. Sokolov, Alexey E. Alexandrov, Maria A. Kniazeva, Ivan Yu. Eremchev, Andrey V. Naumov, Danil W. Boukhvalov, Burkhard König, Maria A. Kalinina*

SI. Materials and methods

Materials

Zn(II) meso-tetra(4-pyridyl)-porphine (ZnTPyP) and zinc(II) 5,10,15,20-tetrakis(4-carboxyphenyl)-porphine (ZnTCPP) were synthesized earlier through the procedures described in ref.[1] and ref.[2], respectively. N,N'-di(propanoic acid)-perylene 3,4,9,10-tetracarboxylic diimide (PA-PDI) was synthesized using the protocol reported in ref.[3]

Zinc acetate dihydrate ($Zn(OAc)_2 \cdot 2H_2O$), 2-methylimidazole (2-MeIm), molybdenum disulfide (MoS_2), terephthalic acid (TPA), 1,5-dihydroxynaphthalene (DHN) and triethylamine (TEA) were obtained commercially from Sigma-Aldrich and used without further purification. Singlet Oxygen Sensor Green (SOSG) was obtained commercially from Invitrogen/Molecular Probes. Methanol (Acros) was used as a solvent to prepare ZnTCPP and DHN solutions. Chloroform ("Component-reaktiv", Russia) was purified by distillation over CaH_2 and Al_2O_3 chromatography column and used for preparation of ZnTPyP solutions. For preparation of solutions of $Zn(OAc)_2$, 2-methylimidazole, and 1,5-dihydroxynaphthalene, water was previously deionized to an electrical conductivity of 16 MΩ/cm.

Synthetic procedures

General procedure for synthesis of graphene oxide (GO). GO monolayer sheets was synthesized as described in ref.[4] A 1g-portion of dry graphite powder (Graphenox, GNP 350) was mixed with 1.67 g of potassium persulfate ($K_2S_2O_8$, Sigma-Aldrich, >99%) and 1.67 g phosphorus (V) oxide (P_2O_5, Sigma-Aldrich, >98%) in 8 ml of concentrated H_2SO_4. The mixture was kept at 80 °C for 4.5 hours. After thatthe mixture was cooled to room temperature, diluted with 350 ml of deionized water (DIW), and filtered. The as-peroxidized graphite was washed with DIW and dried at 60-70 °C overnight. Dry peroxidized graphite was redispersed in 40 ml of concentrated H2SO4 in an ice bath. A 5-g portion of potassium permanganate (K_2MnO_4, Reakhim, reagent grade) were added gradually under constant stirring to avoid overheating. The mixture was stirred at 35 for 2 h and then slowly diluted with 80 ml DIW upon cooling in the ice bath. The mixture was stirred additionally for 2 h, and then 250 ml DIW was added, followed by the addition of 6 ml of H_2O_2 (30 wt %, Reakhim, reagent grade) to react with the excess of K_2MnO_4. The oxidized product was filtered and washed with 100 ml HCl (1:10) to remove metal ion impurities, followed by washing with 300 ml of DIW and dialysis to remove acid. An aqueous dispersion of GO was prepared by dispersing the oxidized material in DIW in an ultrasound bath for 2 h.

Fabrication of molybdenum disulfide (MoS_2) one-dimensional particles by the method developed by our group has been reported in ref.[5] Molybdenum disulfide (MoS_2) 0.500 g was added to 15 ml of an aqueous solution containing 11.7 g of 2-methylimidazole (2-MeIm). The solution was sonicated for 4 h under continuous stirring at a temperature of 80 °C by using Ultrasonic homogenizer Vibra-Cell VCX 750. The as-prepared solution was filtered using a Pragopor membrane filter for separation of non-exfoliated MoS_2 sheets from target sol. The dark green filtrate containing MoS_2 nanoflakes was collected and purified from 2-MeIm by repeated centrifugation at 12000 rpm for 10 min and redissolved in pure water several times to achieve a decrease of the pH value from 11.5 down to 5.8–6.2 suggesting a complete removal of 2-MeIm.

Synthesis of ZnTPyP-based SURMOF/GO hybrid material in GO-based Pickering emulsions has been described in detail in our recent publication.[6] The 1.5% w/w aqueous sol of GO (1.7 ml) with lateral particle size of 5 μm and 110 mg of solid zinc (II) acetate dihydrate ($Zn(OAc)_2 \cdot 2H_2O$, Sigma-Aldrich, ≥98%) were dissolved in a 8 ml of a mixture of water and ethanol (90/10). ZnTPyP was dissolved in 10 ml of chloroform to obtain

2.9×10^{-3} M solution. The solutions were mixed in sealed vials, intensively shaken and ultrasonicated for 15 min. Then 0.5 ml of ethanol was added, and the vial was again shaken, ultrasonicated for 15 min and placed into the oven for 48 hours at 70 °C. The obtained powder was filtered, washed with water and methanol several times and dried overnight under vacuum. Black or dark-purple powder was collected. The most essential characteristics of the as-synthesized hybrid photocatalysts are given in Table S1.

Synthesis of PDI-PA/GO composite material has been reported in ref.[7] The 2.5% w/w aqueous solution of graphene oxide (8 mL) with the GO size of 5 μm (Figure S1) and the 0.5 mL of aqueous solution of $Zn(OAc)_2$ (5×10^{-2} M) were mixed in a sealed vial and ultrasonicated for 20 min. Then, 33 mL of aqueous solution of PA-PDI (C=1.4×10^{-5} M) were added into the vial; the mixture was shaken and placed into the oven for 24 h at 70 °C. The obtained black powder was filtered, washed with water and methanol several times, and dried overnight under a vacuum. The properties of the synthesized hybrid photocatalysts are summarized in Table S1.

Synthesis of ZnTCPP-based SURMOF/MoS2 hybrid material by using a solvothermal protocol developed by our group has been reported in ref.[8] Aqueous solution of $Zn(OAc)_2$ (V = 1.5 mL, C = 10^{-3} M) was added to aqueous sol of MoS_2 (V = 12 mL, C = 3 g/L). The mixture was sonicated in a Stegler 3DT ultrasonic bath (120 W) for 30 min at 25 °C. Then the 37.5 mL portion of methanol solution of ZnTCPP (C = 10^{-5} M) was added to the as-prepared hydrosol and placed in an oven at 80 °C for 48 h. The resulting pale-green precipitate was filtered off and washed with water and methanol, and then the precipitate was dried using an ERSTEVAK EV-DF18SA-TPM lyophilic drying system. The main characteristics of the synthesized hybrid photocatalysts are given in Table S

Methods

X-ray photoelectron spectroscopy (XPS). The surface state and electronic structure of graphene oxide monolayer were investigated by XPS (Kratos AXIS UltraDLD ultrahigh vacuum system for surface analysis) using Al*K*α radiation (1486.6 eV) as a probe. Transmission energy was 15 eV and the step of recording the reference spectrum was 1 eV, while the steps for C1*s*, O1*s*, and Si2*p* spectra were equal to 0.1 eV. The spectra were processed using the CasaXPS software package. The spectra were corrected with respect to the position of the sp^2 carbon line (284.6 eV). The deconvolution was carried out as the superposition of the Gaussian and Lorentz functions in the 50/50% proportion (GL (50)), and the background was subtracted according to Shirley.

C/O ratios were calculated as the ratio of the area under the 1s curve of the carbon spectrum to the area under the 1s curve of the oxygen spectrum. The contribution to the oxygen spectra from silicon oxide was taken into account (the concentration of oxygen 'bound' to Si was calculated from the area of the oxide component of the 2p Si spectrum and subtracted from the 1s O spectrum) based on the ratio of 2 oxygen atoms to 1 silicon atom (chemical formula SiO_2). The second way to estimate the C/O ratio is the ratio of the area under the C-C and C=C peak to the sum of the areas of the C-O(OH) and C=O peaks. The calculations are presented in the table S2.

UV-Vis spectra of solutions were recorded in 1 cm quartz cells by using Jasco V-760 spectrophotometer (Spectra Manager™).

X-ray diffraction (XRD) patterns were obtained using an Empyrean (Panalytical) diffractometer equipped with a 1-D position-sensitive X'Celerator detector. Ni-filtered Cu Kα-radiation was employed. Standard Bragg-Brentano (reflection) geometry was employed, allowing the acquisition of out-of-plane diffraction.

Hydroxyl radical probing was performed by measuring fluorescence of terephthalic acids monohydrate ion (TPA-OH). Fluorescence of the aqueous solution of terephthalic acid (TPA) with hybrid photocatalyst (SURMOF/GO) was recorded in a 1×1 cm^2 quartz cell by using Jasco spectrofluorometer model - FP-8350 with 312 nm excitation and 426 nm emission wavelength (Spectra Manager™). Usually, 5 mg of powder was added to the 5 ml solution (TPA, C= 1×10^{-5} M). The solution of TPA was equilibrated with the powders for sorption within 12 hours and then irradiated for 15 min with xenon lamp, equipped with a yellow cut-off filter (>420 nm) and then 3 ml aliquot was taken and centrifuged for 1 min to analyze. In case of analysis in an inert atmosphere the sample was additionally purged with argon.

Photodegradation Studies. For investigating of photocatalytic activity of the SURMOF/GO, PDI-PA/GO and SURMOF/MoS_2 hybrid materials reaction of 1,5-dihydroxynaphthalene (DHN, Sigma-Aldrich, ≥97%) photodestruction was used. Typically, a portion of 10 mg of dry powder of the studied photocatalyst was added to 10 ml of the water/methanol solution (98%/2% v.v.) of DHN (C=1×10^{-4} M). The vial was sealed, shaken and stored in the dark overnight. Then, the samples were put into the quartz cuvette with an optical path of 10 mm and irradiated with a xenon lamp with AM 1.5G filter with irradiance 426 mW/cm^2 (Figure S2), equipped with a yellow cut-off filter (>420 nm). For the experiments performed under an inert atmosphere, the samples were additionally bubbled with argon for 20 min. Decomposition kinetics of DHN was studied spectroscopically by measuring the integral relative decrease of intensity of the DHN absorption bands at 298 nm in all experiments both with and without applied EEF. For this purpose, 100 μl of the reaction solution was taken only every 10 minutes to avoid additional perturbations and then added to a 2 ml water/methanol solution (98%:2%v.v.). The spectra of the as-prepared probes were recorded on a Shimadzu UV-2450 dual-beam spectrophotometer in a 1 mm quartz cuvette in the range 200-600 nm. To measure the photocatalytic activity under the applied EEF, the samples were placed in the electrical cell consisting of a capacitor with electrodes made of ITO tightly fitted to the sides of the cuvette, which was attached to a high-voltage DC power source. The reaction was carried out without stirring for a more accurate assessment of a contribution of EEF. The temperature of the reaction mixture was measured before and after photocatalytic degradation using a custom-engineered and previously calibrated thermocouple. All kinetic measurements were carried out at an applied voltage of 4 kV, which corresponds to the maximum achievable value below that of voltage breakdown for this construction. The kinetic dependencies reported herein was reproduced 3-5 times using a new portion of each photocatalyst and freshly prepared solutions of DHN for every next run of experiments. The experimental error was estimated by conventional calculations for each set of the as-obtained experimental data for various regimes (EEF-free aerobic of anaerobic, EEF-assisted aerobic of anaerobic, respectively).

Time-resolved photoluminescence spectroscopy. The dry powder of SURMOF/GO photocatalyst was fixed on a thin non-luminescent glass substrate with a thin viscous polyisobutylene (PIB) toluene solution layer or placed into a thin optically clear cuvette containing either distilled water or a 1,5-dihydroxonaphthalene solution. To vary the electric field strength, the sample is placed in a capacitor (the distance between the plates is 10 mm, the value of the field varies from 0 to 200 kV/m). The capacitor with the sample is placed into a luminescent microscope on a controlled piezo driven stage (NanoScanTech). The SURMOF/GO particles are excited using a femtosecond parametric laser system TOPOL (Avesta) at 400 nm (SHG from 800 nm), pulse duration ~200fs, 1 MHz repetition rate. The laser beam is focused and the luminescence signal is collected using a large working distance (13 mm) microscope objective Mitotoya (M Plan Apo SL, 100x, NA 0.55). Using the large working distance objective with high numerical aperture allows us to reach the sample inside the condenser as well as achieve a high spatial resolution. Separation of laser radiation and luminescence signal is performed using an interference optical filter (Semrock). A high-sensitivity cooled EMCCD-camera (Andor iXon Ultra, cooling to -80 ºC) is applied to record luminescence images of photocatalyst particles. Spectra and photoluminescent kinetics are registered from the diffraction-limited region of the sample (~300 nm). Spectra are recorded by an imaging spectrometer (SOL Instruments MS520). Photoluminescent kinetics are measured by a single-photon avalanche diode (SPAD) MPD (MicroPhoton Devices, (time resolution - 100 ps, QE ~ 35% at 630 nm) with TSCPS electronics (Becker&Hickl DPC 230, time resolution – 165 ps).[9]

Gas chromatography–mass spectra were acquired with "Aglilent 7890B MSD5977B", column DB5-MS 15m, 0.25 mm, 0.25 μm. Gas - He, flow rate 1 ml / min. Injector 280 °C. The initial temperature of the thermostat 80 °C is held for 1.5 min, then heated to 310 °C at a rate of 15 °C/ min maximum the temperature is held for 10 minutes. The injection volume is 1 μL. Splitting the stream 10 to 1. Sample preparation: the sample was evaporated in a vacuum rotary evaporator at 45 °C and derivatized using BSTFA at 80 °C for 15 min.

DFT calculations were performed using QUANTUM-ESPRESSO pseudopotential code,[10] employing the generalized gradient approximation[11] for exchange-correlation potential in a spin-polarized mode. A full optimization of lattice constants and atomic positions was carried out. During optimization, the electronic ground state was consistently found using ultra-soft pseudopotentials.[12] The value of the cut-off energy is 25 Ry for all calculations. The forces and total energies were optimized with accuracies of 0.04 eV Å−1 and 1.0 meV/supercell, respectively. The densities of states plot were conducted with a 6×6×1 Monkhorst-Pack k-point grid for the Brillouin zone sampling.[13] Semiempirical calculation of the bandgap was performed by the formula:

$E_{gap} = 1.1 \cdot E_{DFT} + 0.8$ eV,

where E_{DFT} is the bandgap calculated within the standard DFT framework (for details, see ref.
[14]).

X-ray diffraction (XRD) patterns were obtained using Empyrean (Panalytical) diffractometer equipped with 1-D position-sensitive X'Celerator detector. Ni-filtered Cu Kα-radiation was

employed. Standard Bragg-Brentano (reflection) geometry was employed, allowing acquisition of out-of-plane diffraction.

Characterization of photocatalysts

Table S1. Characterization data for hybrid materials used for the EEF-assisted photocatalytic studies. Taken from [6], copyright (2022), with permission from Elsevier Ltd; [7], free of copyright; [8], copyright (2023), with permission from American Chemical Society.

Hybrid photocatalysts	**2θ, °*a***	**average micropore diameter, nm*b***	**molar percentage of content organic linker in hybrid material, %*c***
GO/SURMOF	5.4, 6.2, 9.0	1.12	7
GO/PDI-PA	21.5, 23.9	-	19
MoS_2/SURMOF	4.5, 8.8, 13.4	1.63	12.6

a obtained by X-ray diffraction studies, for corresponding XRDs, see refs.
b as determined by XRD modeling and BET nitrogen absorption measurements, for details, see refs.
c data obtained by thermogravimetric analysis, for corresponding TGA curves, see refs.

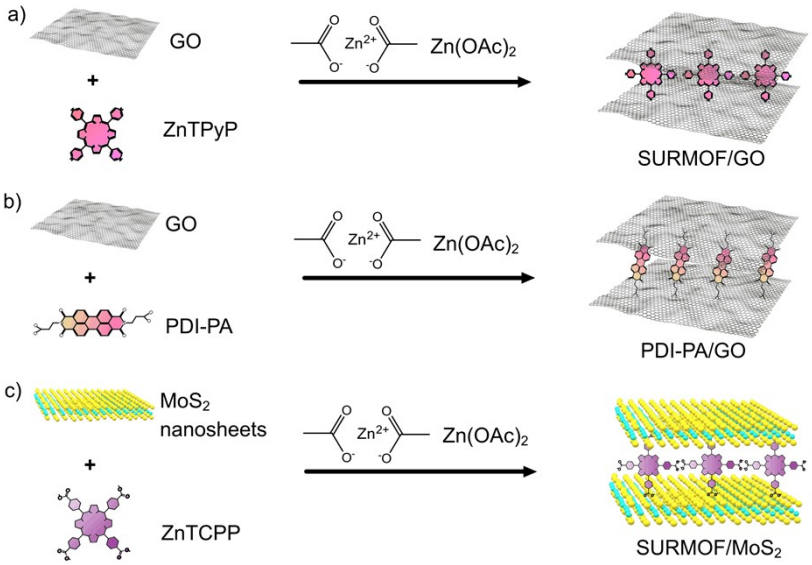

Figure S1. Schematically illustrated structures of (a) SURMOF/GO hybrid, (b) PDI-PA/GO composite, and (c) SURMOF/MoS_2 hybrid material.

SII. Characteristics of EEF cell

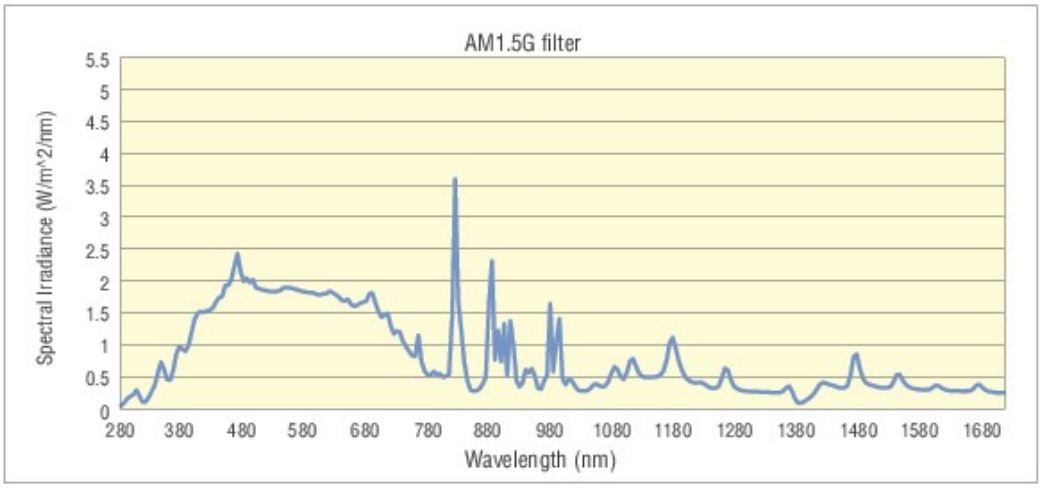

Figure S2. Extinction spectra of xenon lamp with AM1.5G filter.

Thermal effect of EEF

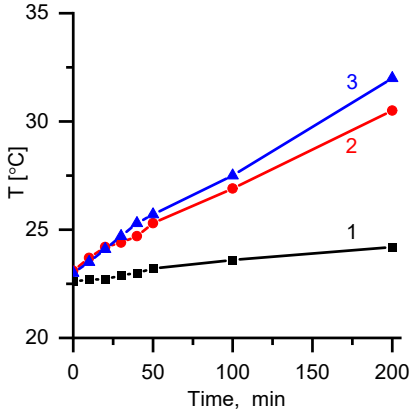

Figure S3. Time dependencies of temperature of water in the EEF-cell in the presence of pure GO in 1-light-off/EEF-on, 2-light-on/EEF-off and 3- light-on/EEF-on modes.

DHN adsorption on GO under applied EEF

To assess the effect of EEF on the adsorption of DHN on GO, the blank experiment with a non-modified GO in the 1×10^{-4} M solution of DHN in the as-constructed setup with and without applied voltage was carried out. The difference in the decrease of intensity of the main absorption band of DHN at 298 nm did not exceed 5% suggesting that EEF does not significantly influence the adsorption of the organic substrate upon polarization of the GO matrix in water (Figure S4).

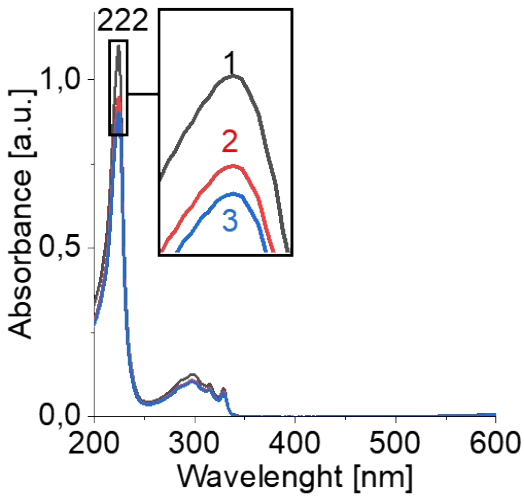

Figure S4. UV−vis spectra recorded for DHN aqueous solution (10^{-4}M) in a presence with a pure GO powder (aerobic mode): 1 - starting solution of DHN; 2- EEF-off, 3 – EEF-on. The sorption experiments were continued for 30 min.

EEF effect on visible-light photocatalytic properties of non-sensitized GO

EEF does not promote its own photocatalytic activity of a non-sensitized GO with respect to DHN in the presence of oxygen as well as in the argon-rich solution irradiated at λ>420 nm (Figure S5). That is, the application of EEF does not enhance the semiconductor behavior of GO as a potential photocatalyst at least under its irradiation with visible light.

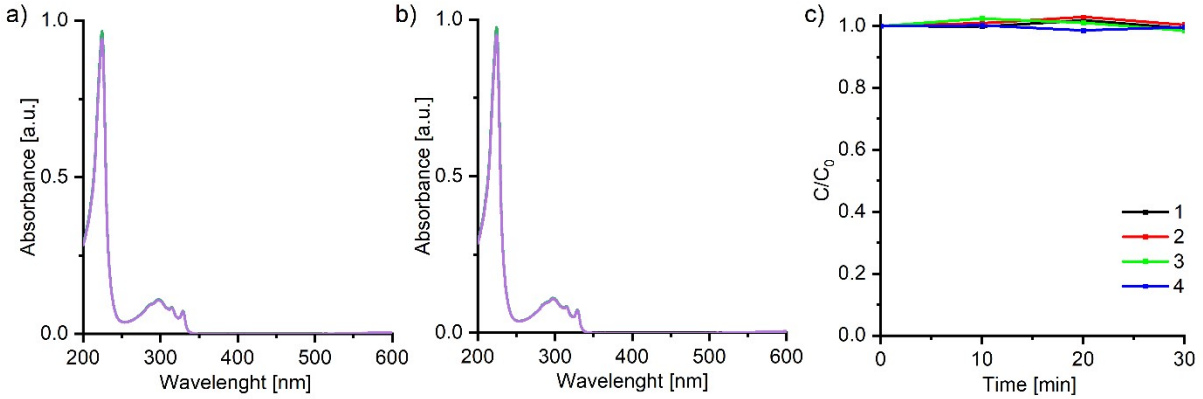

Figure S5. UV−vis spectra recorded for aerobic photodegradation of DHN in the aqueous solution with pure GO powder in (a) EEF-on and (b) EEF-off regimes. (c) Kinetics of photodegradation in different regimes: aerobic EEF-off (1); aerobic EEF-on (2); anaerobic EEF-off (3); and anaerobic EEF-on (4).

SIII. Ultra-fast time resolved photoluminescence spectroscopy

Experimental setup

The influence of EEF on photochemistry of the organic components of our GO-based hybrids was studied for the ZnTPyP SURMOF/GO hybrid by using ultrafast time-resolved photoluminescence spectroscopy setup equipped with the fluorescence microscope (Figure S6).

The measurements of spectral response of ZnTPyP to the applied EEF were carried out in the air (Figure S7), in distilled water (Figure S8) and in the 1×10^{-4} M solution of DHN (Figure S9).

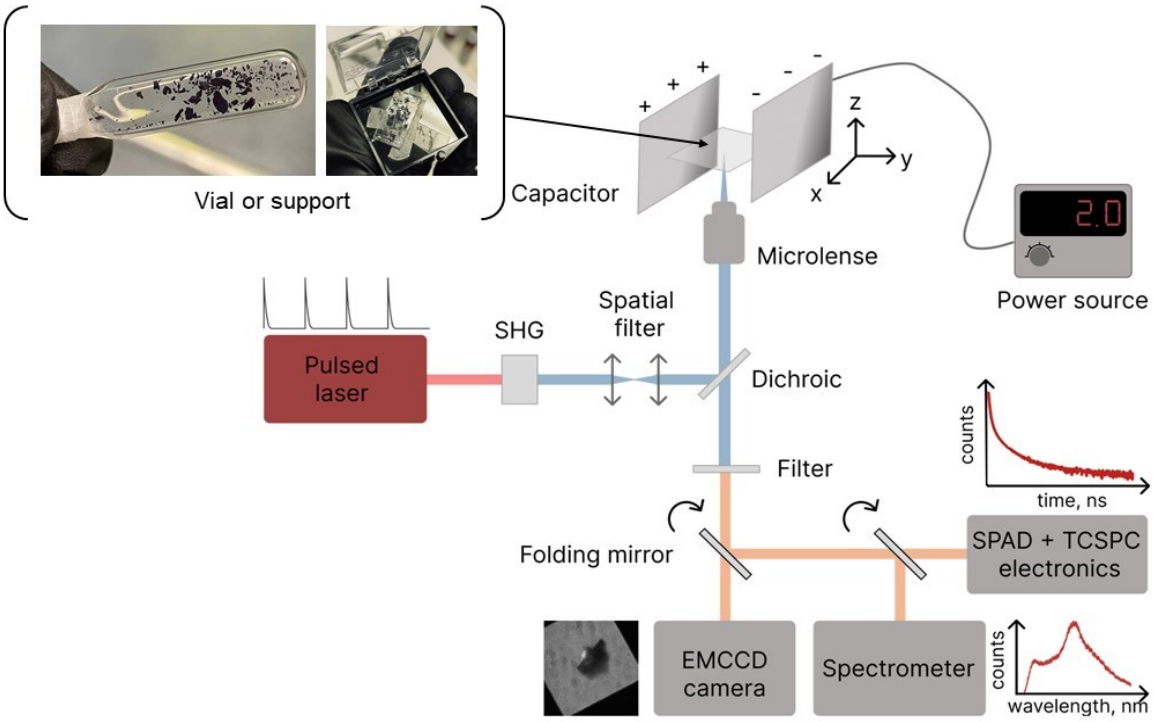

Figure S6. Schematically illustrated studies of the EEF effect of photochemistry of the SURMOF/GO hybrid by using ultrafast time-resolved photoluminescence spectroscopy setup equipped with the fluorescence microscope.

EEF effect on photochemistry of porphyrin sensitizer

The control experiments without EEF were carried out under similar conditions. Figure S7a shows the luminescence microphotograph of the ZnTpyP-based SURMOF/GO hybrid particle exhibiting strong fluorescence due to the ordering of porphyrins into the MOF clusters that prevents contact quenching between ZnTPyP and GO. Figure S7b and S7c show the fluorescence spectra and fluorescence decay curves recorded for the same hybrid material in the air in the EEF-on (red) and EEF-off regimes (black), respectively. We did not find significant difference in the optical behavior of ZnTPyP in the hybrid under applied EEF with respect to that under standard EEF-free conditions. The same results were obtained with this hybrid material in the aqueous media (Figs. S8 and S9). These observations suggest that EEF does not influence the photochemical properties of the porphyrin even in the media with the lowest dielectric constant.

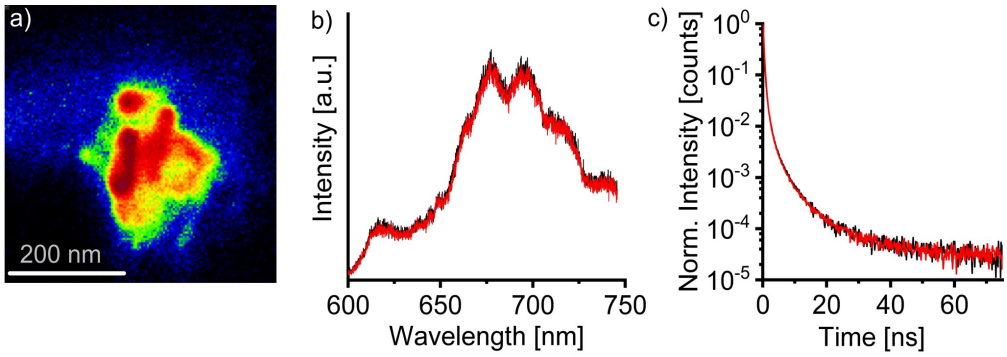

Figure S7. a) Luminescence image of the SURMOF/GO photocatalyst particle; b) spectra and c) kinetics of photoluminescence decay in EEF-off (black) and EEF-on (4kV) regimes, respectively.

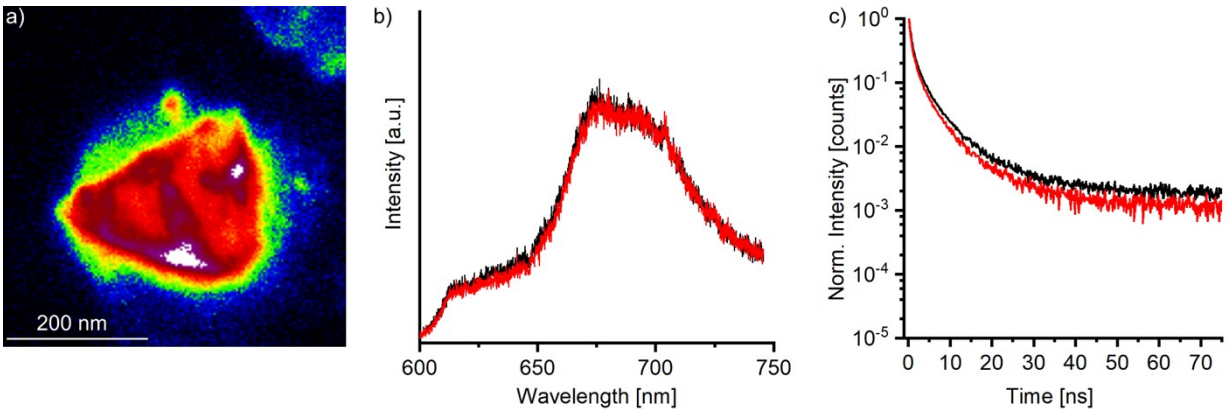

Figure S8. a) Photoluminescence image of the SURMOF/GO particles dispersed in distilled water; b) spectra and c) kinetics of photoluminescence decay in EEF-off (black) and EEF-on (red) regimes.

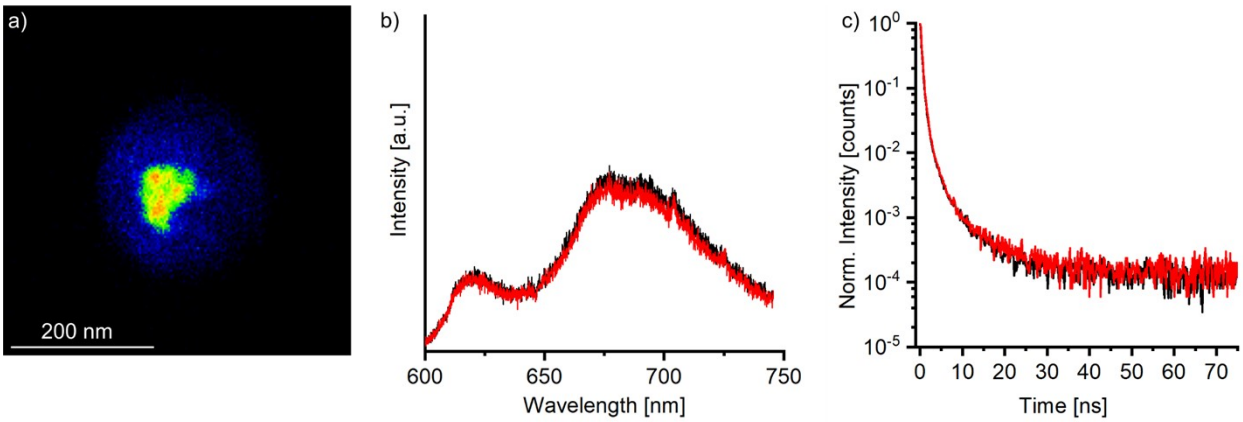

Figure S9. a) Photoluminescence image of photocatalyst particles in 10^{-4}M solution of DHN; b) spectra and c) kinetics of photoluminescence decay in EEF-off (black) and EEF-on (red) regimes.

SIV. Kinetics and mechanism of EEF-assisted photocatalytic degradation of DHN

Fluorescence probe of hydroxyl radicals in EEF

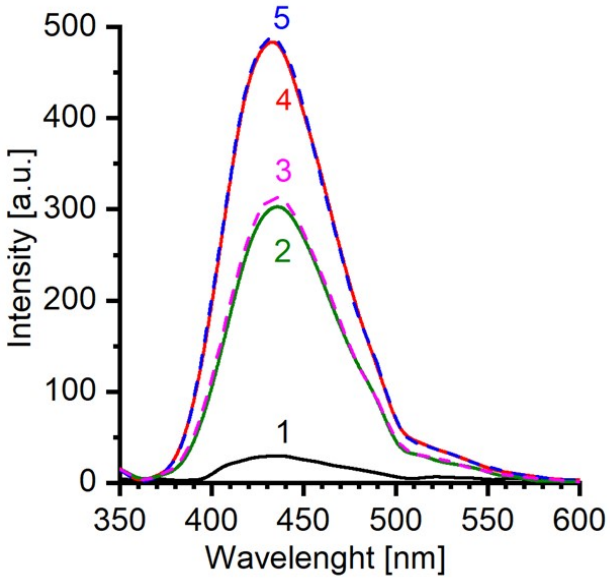

Figure S10. Fluorescence spectra of aqueous solution of TPA (C = 10^{-5} M) over GO/ZnTPyP hybrid before (1) and after 15 min irradiation at λ_{ex} = 440 nm under aerobic (2, 3) and in anaerobic (4, 5) conditions. The pairs of spectra (2, 4) and (3, 5) were recorded in EEF-off and EEF-on regimes, respectively.

Complete kinetic dependencies of photodegradation of DHN with SURMOF/GO

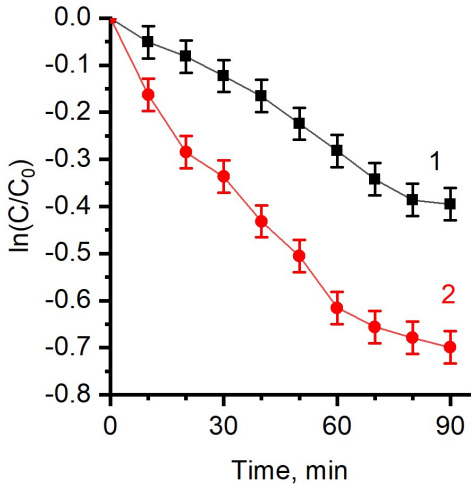

Figure S11. Kinetics of aerobic photodegradation of DHN (10^{-4} M) in the aqueous solutions with the SURMOF/GO hybrid in EEF-off (curves 1) and EEF-on (curves 2) regimes. The kinetic dependencies were plotted using the values of the absorption decrease at λ=298 nm.

Mechanism of photodegradation of DHN with photocatalysts in a static EEF cell

The possible influence of EEF on the chemistry of the reaction products was preliminary assessed via the analysis of the supernatant solutions by UV-vis spectroscopy and GC-MS after the reactions were completed. Yuglon, a well-known product of photooxidation/photoinduced hydroxylation of DHN, formed in the reaction solutions in the presence of the SURMOF/GO hybrid upon intense mixing was found both by UV-vis and mass-spectrometry. However, we did not observe characteristic absorption of Yuglon at 423 nm in the spectral pictures of processes studied herein (Figure S12). The GC-MS analysis showed that a different compound, 5-hydroxytetralin-1,4-dione (HTDO), was formed under the conditions applied in this work (Figure S13 and S14). This compound is a product of hydrogenation of Yuglon via the electron transfer from GO to water. Since HTDO was found in the reaction mixtures both in EEF-off and EEF-on regimes (Figure S13, S14), such sequential oxidation-reduction reactions can occur on the surface of the hybrid photocatalyst because the desorption of products is slow in the absence of stirring. That is, the chemical pathways of photodestruction of DHN predominantly depend on the chemistry of intermediates generated by the hybrid material in combination with the applied convection regime rather than on the effect of EEF.

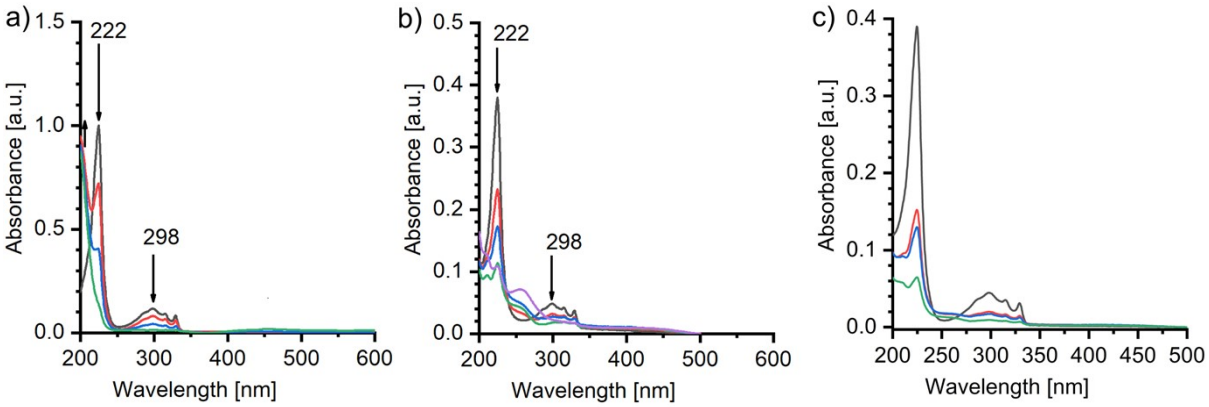

Figure S12. Typical UV−vis spectra of photodegradation of DHN in aqueous solution assisted by (a) SURMOF/GO, (b) PDI-PA/GO and (c) SURMOF/MoS_2 hybrid materials in EEF-on regime.

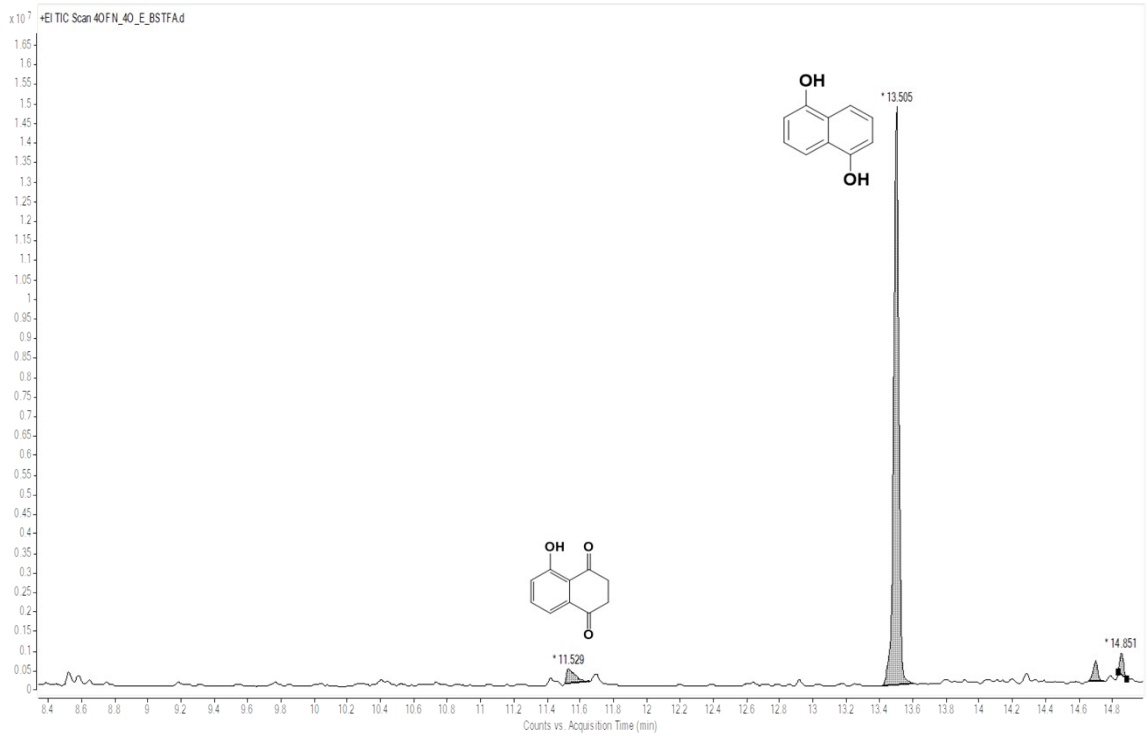

Figure S13. GC-MS pattern of supernatant after photobleaching of DHN assisted by the SURMOF/GO material in the oxygen-rich solutions in EEF-off regime.

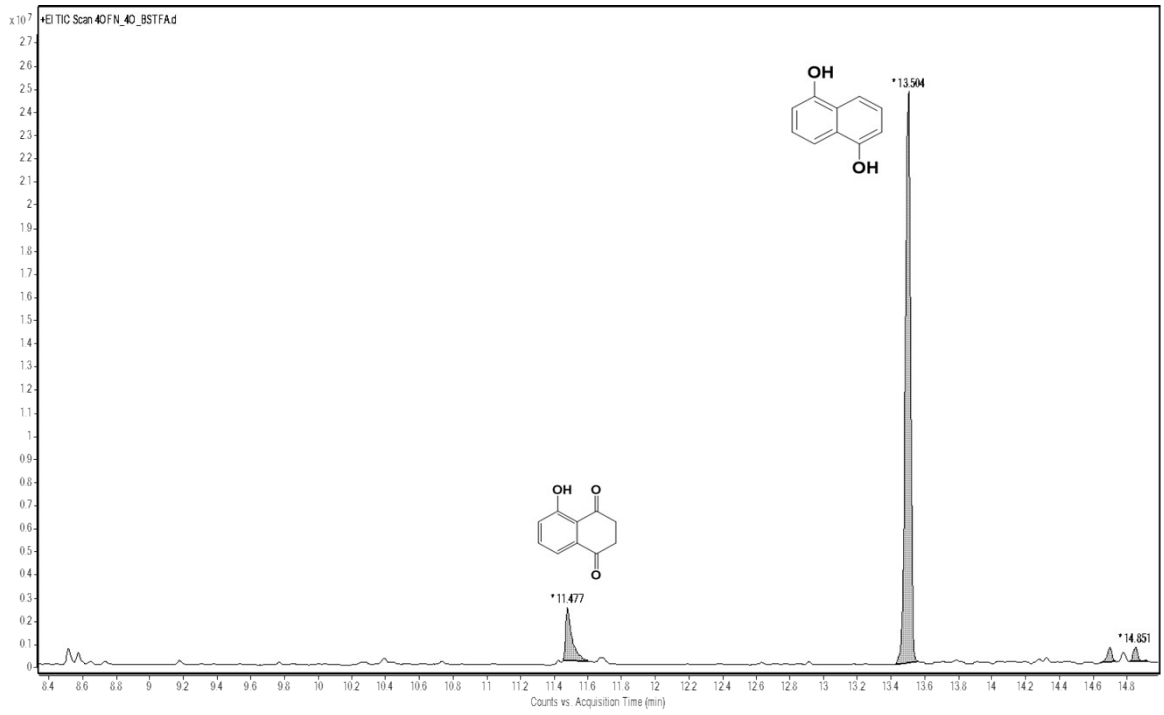

Figure S14. GC-MS pattern of supernatant after photobleaching of DHN assisted by the SURMOF/GO material in the oxygen-rich solution in EEF-on regime (4kV).

SV. XPS analysis of GO

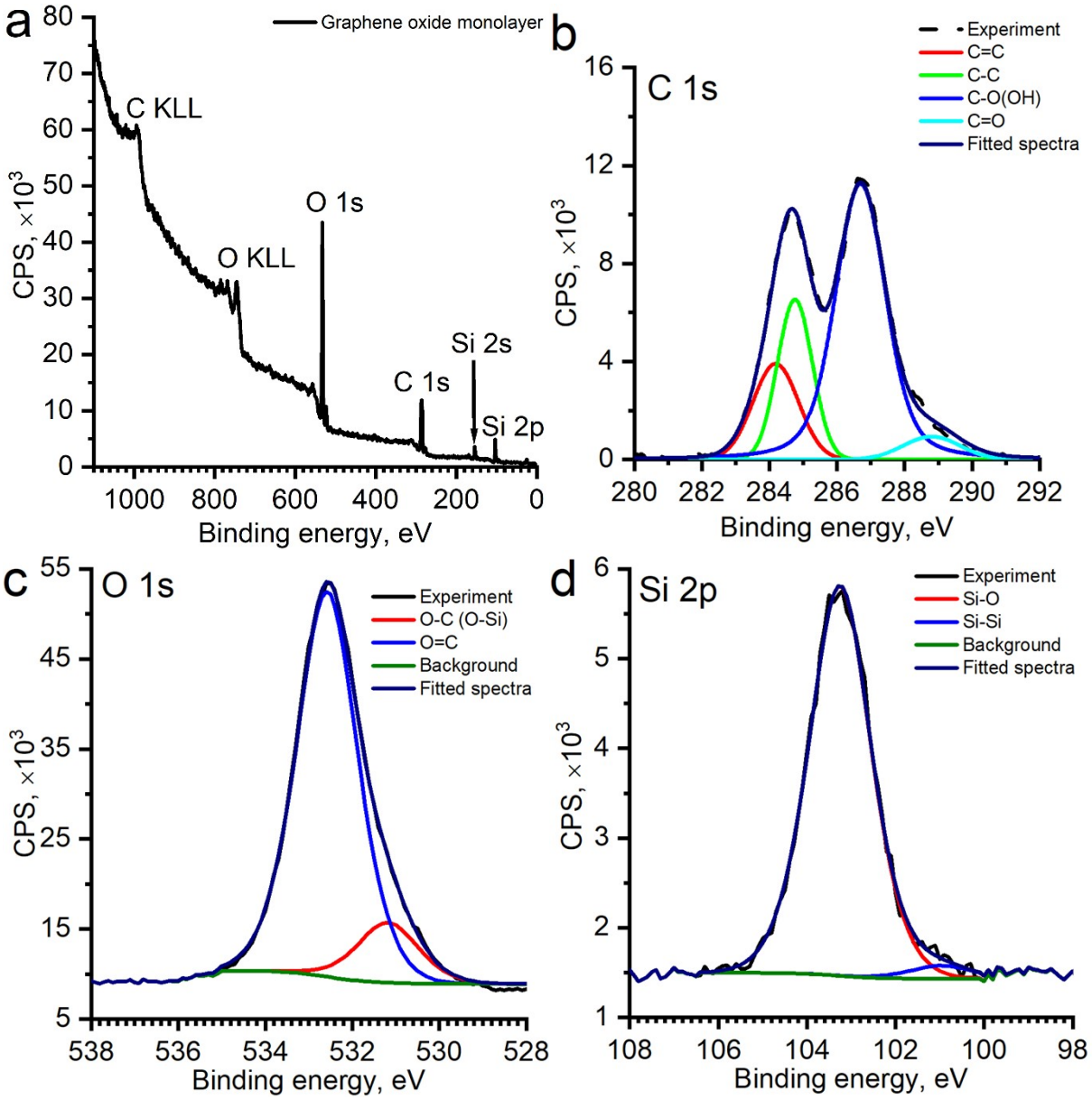

Figure S15. a) XPS spectrum of GO monolayer and fitting results of b) C 1s, c) O 1s, d) Si 2p.

Table S2. Calculations of C/O ratio in graphene oxide monolayer.

Name	Eb, eV	R.S.F.	Area	Area Norr	$\frac{\text{SumC}}{\text{SumO}}$	$\frac{C-C}{(C-O(OH))+(C=O)}$
O1s		2,85	96348,6	15421,79	2,534	
C1s		1	39076,7	39076,7		
O-Si		0,865	7951,4	9192,37		
C-C	284,6		17357,7			0,805

C-O(OH)	286,77		19475,3			
C=O	288,7		2092			

SVI. DFT modeling and XRD analysis

DFT modeling of GO and MoS_2

Based on a previously developed model of GO[14] and C:O ratio revealed by XPS (see Figure S12), the structure shown in Figure 7a has been proposed as a model. This model system consists of an almost entire oxidized area and non-oxidized channels of carbon atoms with sp^2 hybridization. Despite the presence of these large non-oxidized areas, this system is a semiconductor with a distinct bandgap (see Figure 3b).

Applying the field of 200 kV/m applied along the GO sheet provides insignificant changes in the work functions (0.113 eV and 0.120 eV for the field applied along and across channels, respectively). Since in the presence of the field along the c axis leads to the absence of saturation of the vacuum potential (see Figure S16), we cannot calculate the work function. However, we can estimate changes in the electrical properties of GO by calculating the distance from the center of the graphene flat corresponding with zero difference between values of Fermi energy and vacuum potential. In the absence of an external field, this value is about 2.5 Å, which corresponds with the location of the electrons of hydrogen atoms in hydroxyl groups. Applying an out-of-plane electric field of 200 kV/m increases the discussed value up to 14.4 Å, corresponding with a significant electron density shift far from the nuclei (see Figure 3e).

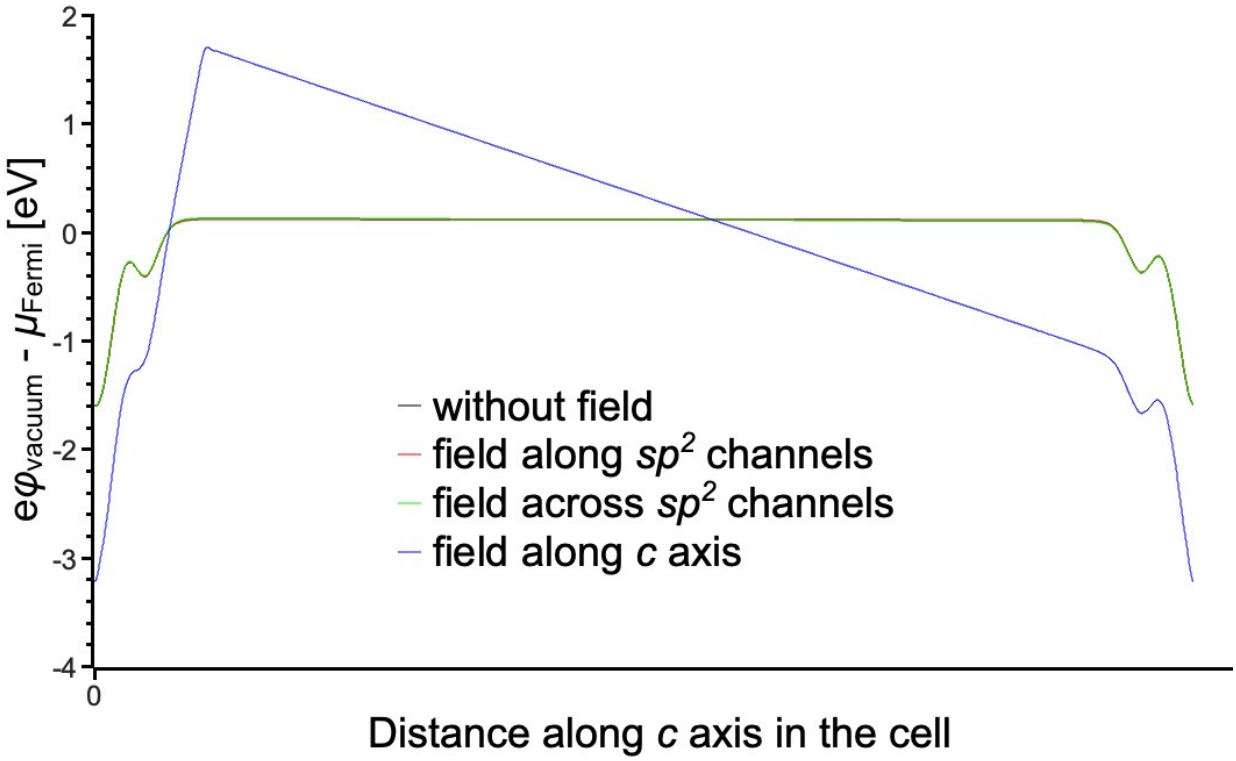

Figure S16. Vacuum potential referenced to the Fermi energy plotted against the distance along *c* axis.

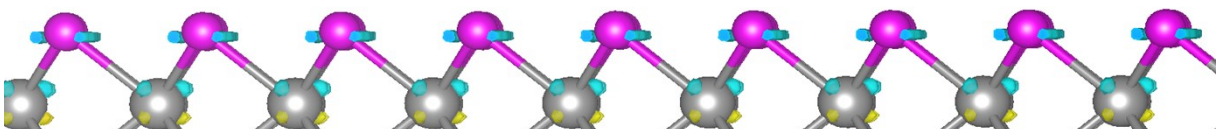

Figure S17. The charge densities change after applying the electric field along the *c*-axis of MoS_2 monolayer. The yellow and cyan "clouds" indicate an increase and decrease in electron density. Mo atoms are depicted in light grey, and S atoms are shown in magenta. The background cut-off (isosurface level) is 0.01 $e^-/Å^3$, the same as in Fig. 3 in the main text.

XRD analysis

Additionally were investigated the influense of EEF on the structure of SURMOF/GO hybrid (FigS18). The SURMOF/GO materials can be reused several times without changing their structure by the EEF.

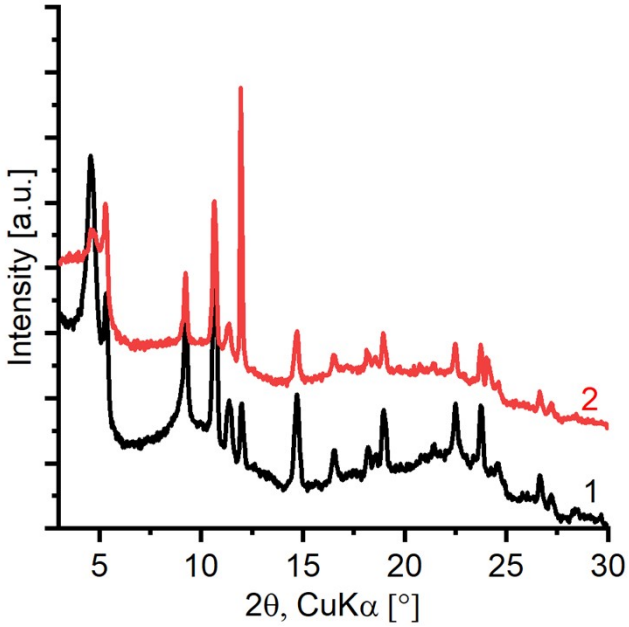

Figure S18. X-ray diffractogram of the SURMOF/GO hybrid recorded before(1) and after (2) using in photooxidation of DHN in EEF-on regime.

References

1 X. Zhou, X. Huang, X. Qi, S. Wu, C. Xue, F. Y. C. Boey, Q. Yan, P. Chen and H. Zhang, *J. Phys. Chem. C*, 2009, 113, 10842–10846.

2 A. D. Adler, F. R. Longo, F. Kampas and J. Kim, *J. Inorg. Nucl. Chem.*, 1970, 32, 2443–2445.

3 A. Datar, K. Balakrishnan and L. Zang, *Chem. Commun.*, 2013, 49, 6894.

4 S. Sladkevich, J. Gun, P. V Prikhodchenko, V. Gutkin, A. A. Mikhaylov, V. M. Novotortsev, J. X. Zhu, D. Yang, H. H. Hng, Y. Y. Tay, Z. Tsakadze and O. Lev, *Nanotechnology*, 2012, 23, 485601.

5 M. R. Sokolov, K. A. Tumbinskiy, A. I. Zvyagina, I. N. Senchikhin, A. A. Averin, A. E. Aleksandrov, A. R. Tameev, A. A. Ezhov and M. A. Kalinina, *Colloid Interface Sci. Commun.*, 2022, 47, 100604.

6 A. G. Nugmanova, E. A. Safonova, A. E. Baranchikov, A. R. Tameev, A. V. Shkolin, A. A. Mitrofanov, A. A. Eliseev, I. N. Meshkov and M. A. Kalinina, *Appl. Surf. Sci.*, 2022, 579, 152080.

7 M. Sokolov, A. Nugmanova, A. Shkolin, A. Zvyagina, I. Senchikhin and M. Kalinina, *J. Compos. Sci.*, 2023, 7, 14.

8 M. R. Sokolov, K. A. Tumbinskiy, E. A. Varlamova, A. A. Averin, A. V. Shkolin and M. A. Kalinina, *ACS Appl. Mater. Interfaces*, 2023, 15, 49299–49311.
9 I. Y. Eremchev, M. Y. Eremchev and A. V Naumov, *Physics-Uspekhi*, 2019, 62, 294–303.
10 P. Giannozzi, O. Andreussi, T. Brumme, O. Bunau, M. Buongiorno Nardelli, M. Calandra, R. Car, C. Cavazzoni, D. Ceresoli, M. Cococcioni, N. Colonna, I. Carnimeo, A. Dal Corso, S. de Gironcoli, P. Delugas, R. A. DiStasio, A. Ferretti, A. Floris, G. Fratesi, G. Fugallo, R. Gebauer, U. Gerstmann, F. Giustino, T. Gorni, J. Jia, M. Kawamura, H.-Y. Ko, A. Kokalj, E. Küçükbenli, M. Lazzeri, M. Marsili, N. Marzari, F. Mauri, N. L. Nguyen, H.-V. Nguyen, A. Otero-de-la-Roza, L. Paulatto, S. Poncé, D. Rocca, R. Sabatini, B. Santra, M. Schlipf, A. P. Seitsonen, A. Smogunov, I. Timrov, T. Thonhauser, P. Umari, N. Vast, X. Wu and S. Baroni, *J. Phys. Condens. Matter*, 2017, 29, 465901.
11 J. P. Perdew, K. Burke and M. Ernzerhof, *Phys. Rev. Lett.*, 1996, 77, 3865–3868.
12 D. Vanderbilt, *Phys Rev B*, 1990, 41, 7892–7895.
13 H. J. Monkhorst and J. D. Pack, *Phys. Rev. B*, 1976, 13, 5188–5192.
14 D. W. Boukhvalov and V. Yu. Osipov, *Chemosensors*, 2022, 10, 480.